

A Non-Stationary Geometry-Based Stochastic Model for MIMO High-Speed Train Channels

(Invited Paper)

Ammar Ghazal¹, Cheng-Xiang Wang^{5,1}, Harald Haas², Mark Beach³, Raed Mesleh⁴, Dongfeng Yuan⁵, Xiaohu Ge⁶, and Mohamed Khaled Chahine⁷

¹Joint Research Institute for Signal and Image Processing, Heriot-Watt University, Edinburgh EH14 4AS, UK.

²Joint Research Institute for Signal and Image Processing, University of Edinburgh, Edinburgh EH9 3JL, UK.

³Department of Electrical & Electronic Engineering, University of Bristol, Bristol BS8 1UB, UK.

⁴Sensor Networks and Cellular Systems (SNCS) Research Center, University of Tabuk, 71491, Tabuk, Saudi Arabia.

⁵School of Information Science and Engineering, Shandong University, Jinan, 250100, China.

⁶Department of Electronics and Information Engineering, Huazhong University of Science and Technology, Wuhan 430074, Hubei, China.

⁷Faculty of Mechanical and Electrical Engineering, Damascus University, Damascus, Syria.

Email: {ag289, cheng-xiang.wang}@hw.ac.uk, h.haas@ed.ac.uk, m.a.beach@bristol.ac.uk, rmesleh.snscs@ut.edu.sa, dfyuan@sdu.edu.cn, xhge@mail.hust.edu.cn, khalidsh@scs-net.org

Abstract—In this paper, a non-stationary wideband geometry-based stochastic model (GBSM) is proposed for multiple-input multiple-output (MIMO) high-speed train (HST) channels. The proposed model employs multiple confocal ellipses model, where the received signal is a superposition of the line-of-sight (LoS) and single-bounced rays. Because of the time-varying feature of angles of arrival (AoAs), angles of departure (AoDs), and LoS angle, the proposed GBSM has the ability to investigate the non-stationarity of HST environment caused by the high speed movement of the receiver. From the proposed model, the local spatial cross-correlation function (CCF) and the local temporal autocorrelation (ACF) are derived for different taps. Numerical results and analysis show that the proposed channel model is capable of characterizing the time-variant HST wireless channel.

I. INTRODUCTION

As a fast and convenient public transportation system, high speed railways have experienced a lot of attentions recently. This has led to a rapid development and implementation of these systems around the world. With the increase in the speed of trains, existing wireless communication systems face several challenges such as fast handover [1], high penetration losses, limited visibility in tunnels, varying Doppler, delay, and angular spreads. Railway communication systems need to overcome these challenges to provide reliable communications and satisfy the growing demand of broadband services from HST passengers. The widely used Global System for Mobile Communication Railway (GSM-R) can only provide a data rate of less than 200 kbps [2], besides the fact that GSM-R is mainly used for train control rather than providing communications for train passengers. Therefore, GSM-R cannot meet the requirements for future high speed data transmissions and International Union of Railways recommended that GSM-R has to be replaced by Long Term Evolution Railway (LTE-R) which is a broadband railway wireless communication system based on LTE-Advanced (LTE-A) [3]. However, both systems

adopt conventional cellular architecture that leads to a spotty coverage and high penetration losses of wireless signals traveling through the metal carriages of HSTs [4]. This problem can be avoided by using mobile relay station (MRS) (or Mobile Femtocell) technology [5]. Dedicated MRSs are deployed on the surface of the train to extend the coverage of the outdoor base station (BS) and reduce the number of dropped calls. It can also reduce the effect of the frequent handover by performing a group handover with the MRS instead of dealing with the individual handover of each passenger [6]. This promising technology has been adopted by IMT-Advanced (IMT-A) [7] and WINNER II [8].

Demonstrating the feasibility of those systems before implementation is not possible without accurate channel models that are able to mimic the key parameters of wireless channels, such as the non-stationarity, in HST scenarios. Several measurement campaigns for HST environments have been conducted but they mainly focused on large scale parameters, like path losses and delay spread and ignored other propagation characteristics [9]. Channel models in the literature have also failed to demonstrate the different propagation parameters of wireless channels in high velocity scenarios. Without using the MRS technology for HST scenarios, the LTE-A system [3] provided a relatively simple single-path fast fading channel model. In [10], the propagation channels between HSTs and fixed BSs were modeled using the ray-tracing method which incorporates a detailed simulation of the actual physical wave propagation process based on Maxwell equations. However, the implementation of ray-tracing models always requires extensive computational resources.

In both the rural macro-cell (RMA) scenario in WINNER II [8] and moving networks scenario in IMT-A channel models [7], the train speed can be up to 350 km/h and the MRS technology is employed. Both channel models assumed that the HST channel satisfies the wide-sense stationary uncorre-

lated scattering (WSSUS) condition which has been proved to be incorrect by measurements [11]. In [9], a non-stationary time-varying GBSM for HST communication systems using MRS was proposed. However, the model only considers the LoS angle and the travel times of the waves between the BS and MRS as time-variant parameters. This paper aims to extend the model in [9] by investigating other time-varying parameters, such as AoAs and AoDs, and deriving other statistical properties, like the local spatial CCF and the local temporal ACF.

The rest of this paper is organized as follows. A GBSM for MIMO HST channels is proposed in Section II. In Section III, the statistical properties of the GBSM are derived. The numerical results and the analysis are presented in Section IV. Finally, the conclusions are drawn in Section V.

II. THE GBSM

We adopt the IMT-A network structure for the HST communication system where MRSs are deployed on the surface of the train. Therefore, the end-to-end communication between the BS and MS will consist of two channels: an outdoor channel between the BS and the MRS and an indoor one that connects the MRS with the MSs inside train carriages as illustrated in Fig. 1. Here, we will focus on the outdoor channel because of the challenges that this channel faces due to the high velocity of the receiver. We consider a MIMO HST communication system with S transmit and U receive omnidirectional antenna elements. The BS is considered to be located on the track-side ($D_{\min} = 50$ m) as in [8]. Both the BS and MRS are equipped with multiple antennas at equivalent heights. Fig. 2 illustrates the geometry of the proposed GBSM, which consists of multiple confocal ellipses with single-bounced rays and the LoS component [12]. For clarity purposes, in this figure, we use a 2x2 MIMO channel model as an example.

Based on the tapped delay line (TDL) structure, the taps are represented by multiple confocal ellipses with the BS and MRS located at the foci where there are N effective scatterers on the i th ellipse (i.e., i th tap), where $i=1, 2, \dots, I$ and I is the total number of ellipses or taps. The semi-major axis of the i th ellipse and the n_i th ($n_i=1, \dots, N$) effective scatterer are denoted by a_i and $s^{(n_i)}$, respectively. The initial distance between the BS and MRS is $D_s = 2f$ with f representing half of the distance between the two focal points of ellipses. The antenna element spacings at the BS and MRS are denoted by δ_T and δ_R , respectively. The multi-element antenna tilt angles are denoted by β_T and β_R . The MRS moves with the train with speed v_R in the direction determined by the angles of motion γ_R . The AoA of the wave traveling from an effective scatterer $s^{(n_i)}$ to the MRS is denoted by $\phi_R^{(n_i)}(t)$. The AoD of the wave that impinges on the effective scatterer $s^{(n_i)}$ is denoted by $\phi_T^{(n_i)}(t)$, while $\phi_{T_p}^{\text{LoS}}(t)$ denotes the AoA of a LoS path. Because of the high speed of the receiver, the HST channel is non-stationary and as a result, the aforementioned channel parameters (i.e., $\phi_R^{(n_i)}(t)$, $\phi_T^{(n_i)}(t)$, and $\phi_{T_p}^{\text{LoS}}(t)$) are time-variant.

Based on the TDL concept, the complex impulse response between the p th ($p=1, \dots, S$) element of the BS, T_p , and the q th ($q=1, \dots, U$) element of the MRS, R_q , can be expressed as $h_{pq}(t, \tau') = \sum_{i=1}^I h_{i,pq}(t) \delta(\tau' - \tau'_i)$, where $h_{i,pq}(t)$ and τ'_i denote the complex time-variant tap coefficient and the discrete propagation delay of the i th tap, respectively. From the above GBSM, the complex tap coefficient for the first tap of the $T_p - R_q$ link is a superposition of the LoS component and single-bounced components, and can be expressed as

$$h_{1,pq}(t) = h_{1,pq}^{\text{LoS}}(t) + h_{1,pq}^{\text{SB}}(t) \quad (1)$$

where

$$h_{1,pq}^{\text{LoS}}(t) = \sqrt{\frac{K_{pq}}{K_{pq} + 1}} e^{-j2\pi f_c \tau_{pq}(t)} \times e^{j[2\pi f_{\max} t \cos(\phi_{T_p}^{\text{LoS}}(t) - \gamma_R)]} \quad (2a)$$

$$h_{1,pq}^{\text{SB}}(t) = \sqrt{\frac{1}{K_{pq} + 1}} \sum_{n_1=1}^N \frac{1}{\sqrt{N}} e^{j(\psi_{n_1} - 2\pi f_c \tau_{pq, n_1}(t))} \times e^{j[2\pi f_{\max} t \cos(\phi_R^{(n_1)}(t) - \gamma_R)]}. \quad (2b)$$

The complex tap coefficient for other taps ($1 < i \leq I$) of the $T_p - R_q$ link is a sum of single-bounced components only and can be expressed as

$$h_{i,pq}(t) = h_{i,pq}^{\text{SB}}(t) = \sum_{n_i=1}^N \frac{1}{\sqrt{N}} e^{j(\psi_{n_i} - 2\pi f_c \tau_{pq, n_i}(t))} \times e^{j[2\pi f_{\max} t \cos(\phi_R^{(n_i)}(t) - \gamma_R)]}, \quad 1 < i \leq I. \quad (3)$$

In (2) and (3), the total power for each tap is normalized to 1, $\tau_{pq}(t) = \varepsilon_{pq}(t)/c$ and $\tau_{pq, n_i}(t) = (\varepsilon_{pn_i}(t) + \varepsilon_{n_iq}(t))/c$ ($i = 1, 2, \dots, I$) are the travel times of the waves through the link $T_p - R_q$ and $T_p - s^{(n_i)} - R_q$, respectively, as shown in Fig. 2. Here, c represents the speed of light and K_{pq} designates the Ricean factor. The phases ψ_{n_1} and ψ_{n_i} are independent and identically distributed (i.i.d.) random variables with uniform distributions over $[-\pi, \pi)$ and f_{\max} is the maximum Doppler frequency with respect to the MRS.

From Fig. 2 and based on the law of cosines, we have

$$\varepsilon_{pq}(t) \approx |D_s - v_R t| - k_p \delta_T \cos \beta_T - k_q \delta_R \cos(\phi_{T_p}^{\text{LoS}}(t) - \beta_R) \quad (4a)$$

$$\varepsilon_{pn_i}(t) \approx \xi_T^{(n_i)}(t) - k_p \delta_T \cos(\phi_T^{(n_i)}(t) - \beta_T) \quad (4b)$$

$$\varepsilon_{n_iq}(t) \approx \xi_R^{(n_i)}(t) - k_q \delta_R \cos(\phi_R^{(n_i)}(t) - \beta_R) \quad (4c)$$

where $k_p = (S - 2p + 1)/2$, $k_q = (U - 2q + 1)/2$, $\xi_T^{(n_i)}(t) = (a_i^2(t) + f^2(t) + 2a_i(t)f(t) \cos \phi_R^{(n_i)}(t)) / (a_i(t) + f(t) \cos \phi_R^{(n_i)}(t))$, and $\xi_R^{(n_i)}(t) = b_i^2(t) / (a_i(t) + f(t) \cos \phi_R^{(n_i)}(t))$ with $f(t) = |f - v_R t|$. Here, $b_i(t)$ denotes the time-varying semi-minor axis of the i th ellipse and is defined by $b_i(t) = \sqrt{a_i^2(t) - f^2(t)}$, where $a_i(t) = |a_i - v_R t|$ and $D_s(t) = |D_s - v_R t|$. Based on the geometric relations in Fig. 3 and similar to the method provided in [13], the time-varying AoA $\phi_R^{(n_i)}(t)$ can be derived and expressed as

$$\phi_R^{(n_i)}(t) = \begin{cases} \gamma_R - \arccos\left(\frac{v_R t - \xi_R^{(n_i)}(t_0) \cos(\gamma_R - \phi_R^{(n_i)}(t_0))}{\sqrt{\xi_R^{(n_i)}(t_0)^2 + (v_R t)^2 - 2\xi_R^{(n_i)}(t_0)v_R t \cos(\gamma_R - \phi_R^{(n_i)}(t_0))}}\right), & 0 \leq t \leq \frac{2D_s}{v_R} \\ \gamma_R + \arccos\left(\frac{v_R t - \xi_R^{(n_i)}(t_0) \cos(\gamma_R - \phi_R^{(n_i)}(t_0))}{\sqrt{\xi_R^{(n_i)}(t_0)^2 + (v_R t)^2 - 2\xi_R^{(n_i)}(t_0)v_R t \cos(\gamma_R - \phi_R^{(n_i)}(t_0))}}\right), & \frac{2D_s}{v_R} < t \leq \frac{4D_s}{v_R} \end{cases} \quad (5)$$

where $\xi_R^{(n_i)}(t_0)$ and $\phi_R^{(n_i)}(t_0)$ denote the initial $s^{(n_i)}$ -MRS distance and the initial AoA, respectively. Note that the AoD $\phi_T^{(n_i)}$ and AoA $\phi_R^{(n_i)}$ are interdependent for single-bounced rays. The relationship between the AoD and AoA for multiple confocal ellipses model can be expressed as [14]

$$\sin \phi_T^{(n_i)}(t) = \frac{b_i^2(t) \sin \phi_R^{(n_i)}(t)}{a_i^2(t) + f^2(t) + 2a_i(t)f(t) \cos \phi_R^{(n_i)}(t)} \quad (6a)$$

$$\cos \phi_T^{(n_i)}(t) = \frac{2a_i(t)f(t) + (a_i^2(t) + f^2(t)) \cos \phi_R^{(n_i)}(t)}{a_i^2(t) + f^2(t) + 2a_i(t)f(t) \cos \phi_R^{(n_i)}(t)}. \quad (6b)$$

The time-variant LoS AoA $\phi_{T_p}^{\text{LoS}}$ can be expressed as [3]

$$\phi_{T_p}^{\text{LoS}}(t) = \begin{cases} \arccos\left(\frac{D_s - v_R t}{\sqrt{D_{\min}^2 + (D_s - v_R t)^2}}\right), & 0 \leq t \leq \frac{2D_s}{v_R} \\ \arccos\left(\frac{-1.5D_s + v_R t}{\sqrt{D_{\min}^2 + (-1.5D_s + v_R t)^2}}\right), & \frac{2D_s}{v_R} < t \leq \frac{4D_s}{v_R} \\ \phi_{T_p}^{\text{LoS}}\left(t \bmod \left(\frac{4D_s}{v_R}\right)\right), & t > \frac{4D_s}{v_R}. \end{cases} \quad (7)$$

III. STATISTICAL PROPERTIES OF NON-STATIONARY HST MIMO CHANNEL MODELS

The statistical characterization of GBSMs for WSSUS MIMO channels has been investigated extensively, e.g., in [15]–[18]. In contrast, only few papers [9], [19], [20] have studied the statistical properties of GBSMs for non-stationary channels [21], [22]. For the proposed non-stationary HST GBSM, we will derive the corresponding correlation properties, i.e., the local spatial CCF and the local temporal ACF.

For non-stationary systems, the local spatial CCF depends on not only the BS and MS antenna element spacings but also time t . Therefore, the local spatial CCF can be expressed as

$$\rho_{pq,p'q'}(t, \delta_T, \delta_R) = \mathbf{E} \{h_{i,pq}(t) h_{i,p'q'}^*(t)\} \quad (8)$$

where $(\cdot)^*$ denotes the complex conjugate operation and $\mathbf{E} \{\cdot\}$ designates the statistical expectation operator.

1) In the case of the LoS component

$$\rho_{pq,p'q'}^{\text{LoS}}(t, \delta_T, \delta_R) = K' e^{j2\pi [P \cos \beta_T - Q \cos(\phi_{T_p}^{\text{LoS}}(t) - \beta_R)]} \quad (9)$$

where $P = (p' - p) \delta_T / \lambda$, $Q = (q' - q) \delta_R / \lambda$, and $K' = \frac{\sqrt{K_{pq} K_{p'q'}}}{(K_{pq} + 1)(K_{p'q'} + 1)}$.

2) In terms of the single-bounced components

$$\rho_{pq,p'q'}^{\text{SB}_i}(t, \delta_T, \delta_R) = \frac{1}{UN} \sum_{n_i=1}^N e^{j2\pi P \cos(\phi_T^{(n_i)}(t) - \beta_T)} \times e^{j2\pi Q \cos(\phi_R^{(n_i)}(t) - \beta_R)} \quad (10)$$

where $U = \sqrt{(K_{pq} + 1)(K_{p'q'} + 1)}$ only appears for the first tap, i.e., $i = 1$.

The local temporal ACF for non-stationary systems depends on the time difference τ and time t and can be expressed as

$$r(t, \tau) = \mathbf{E} \{h_{i,pq}(t) h_{i,pq}^*(t + \tau)\}. \quad (11)$$

1) In the case of the LoS component

$$r^{\text{LoS}}(t, \tau) = \frac{K_{pq}}{1 + K_{pq}} e^{j2\pi v_R \frac{\tau}{\lambda}} e^{j2\pi f_{\max} \cos(\phi_{T_p}^{\text{LoS}}(t + \tau) - \gamma_R) \tau}. \quad (12)$$

2) In terms of the single-bounced components

$$r^{\text{SB}_i}(t, \tau) = \frac{1}{(1 + K_{pq})N} \sum_{n_i=1}^N e^{j2\pi \xi_{T_p}^{n_i}(t, \tau)} \times e^{-j2\pi f_{\max} \cos(\phi_{T_p}^{\text{LoS}}(t + \tau) - \gamma_R) \tau} \quad (13)$$

where $\xi_{T_p}^{n_i}(t, \tau) = \xi_T^{n_i}(t + \tau) - \xi_T^{n_i}(t) + \xi_R^{n_i}(t + \tau) - \xi_R^{n_i}(t)$ and K_{pq} only appears for the first tap.

The statistical properties of the first tap can be easily obtained by substituting (1) into (8) and (11) to get the local spatial CCF and local temporal ACF, respectively.

$$\rho_{pq,p'q'}^1(t, \delta_T, \delta_R) = \rho_{pq,p'q'}^{\text{LoS}}(t, \delta_T, \delta_R) + \rho_{pq,p'q'}^{\text{SB}_1}(t, \delta_T, \delta_R) \quad (14a)$$

$$r^1(t, \tau) = r^{\text{LoS}}(t, \tau) + r^{\text{SB}_1}(t, \tau). \quad (14b)$$

Similarly and based on (3), the local spatial CCF and local temporal ACF of the rest of the taps ($1 < i \leq I$) can be expressed as

$$\rho_{pq,p'q'}^i(t, \delta_T, \delta_R) = \rho_{pq,p'q'}^{\text{SB}_i}(t, \delta_T, \delta_R), \quad 1 < i \leq I \quad (15a)$$

$$r^i(t, \tau) = r^{\text{SB}_i}(t, \tau), \quad 1 < i \leq I. \quad (15b)$$

IV. NUMERICAL RESULTS AND ANALYSIS

In this section, based on the derived local spatial CCF and local temporal ACF in Section III, the statistical properties of the proposed HST MIMO channel model are numerically evaluated and analyzed. Based on the moving networks scenario in [8] that was designed based on some measurements in HST environments, the following parameters were used for the numerical analysis: the carrier frequency $f_c = 6$ GHz, $v_R = 360$ km/h, $f_{\max} = 2$ KHz, $D_s = 500$ m, $D_{\min} = 50$ m, $a_1 = f + 150$ m, $a_2 = f + 180$ m, $\gamma_R = 30^\circ$, and the LoS Ricean factor $K_{pq} = K_{p'q'} = 6$ dB. We use a uniform antenna array with $U = S = 2$ and $\beta_R = \beta_T = 60^\circ$. By adopting a BS antenna element spacing $\delta_T = \lambda$, the absolute value of the local spatial CCF of the non-stationary HST MIMO channel model for the first and second taps are illustrated in Figs. 4 and 5, respectively. In both taps, the local spatial CCF changes with time t due to the non-stationarity of the channel. However, the correlation of the first tap is showing higher values than the

second one because of the LoS component that is dominant in HST scenario [3], [7] and [8].

Figs. 6 and 7 show the absolute values of the local temporal ACF for the first and second taps, respectively. It can be seen from these two figures how the ACF of the proposed non-stationary GBSM varies with time t . Similar to the local spatial CCF, it can be noticed that the LoS component in the first tap will increase considerably the value of the correlation in comparison with the second tap that contains single-bounced components only.

V. CONCLUSIONS

In this paper, we have proposed a non-stationary wideband MIMO HST GBSM for the outdoor channel of HST communication system. Because of its time-varying parameters, the proposed channel model, that takes into account the LoS component and single-bounced rays, enables us to study the time-varying channel statistics. From this model, we have derived the local spatial CCFs and local temporal ACFs for different taps. Numerical results have proved that the stationary assumption is violated for HST channels. They also demonstrated the effect of the LoS component on the correlation properties of the HST channel.

ACKNOWLEDGEMENTS

A. Ghazal acknowledges the sponsorship of his work by Damascus University. The authors would like to acknowledge the support from the RCUK for the UK-China Science Bridges Project: R&D on (B)4G Wireless Mobile Communications. C.-X. Wang thanks the support of the Opening Project of the Key Laboratory of Cognitive Radio and Information Processing (Guilin University of Electronic Technology), Ministry of Education (Grant No.: 2011KF01). R. Y. Mesleh gratefully acknowledges the support from SNCS research center at University of Tabuk under the grant from the Ministry of Higher Education in Saudi Arabia. X. Ge acknowledges the support from the National Natural Science Foundation of China (NSFC) (Grant No.: 60872007 & 61210002), National 863 High Technology Program of China (Grant No.: 2009AA01Z239), the Ministry of Science and Technology (MOST), China, International Science and Technology Collaboration Program (Grant No.: 0903) and Hubei Provincial Science and Technology Department (Grant No.: 2011BFA004).

REFERENCES

- [1] H. Wu, Y. Gu and Z. Zhong, "Research on the fast algorithm for GSM-R switching for high-speed railway," *Journal of Railway Engineering Society*, pp. 92–98, Jan. 2009.
- [2] J. Wang; H. Zhu, and N. J. Gomes, "Distributed antenna systems for mobile communications in high speed trains," *IEEE J. Select. Areas Commun.*, vol. 30, no. 4, pp. 675–683, May 2012.
- [3] 3GPP, TS36.101, V10.2.1, "3rd Generation Partnership Project; Technical Specification Group Radio Access Network; Evolved Universal Terrestrial Radio Access (E-UTRA); User Equipment (UE) radio transmission and reception (Release 10)," Apr. 2011.
- [4] O.B. Karimi, L. J. Liu, and C. Wang, "Seamless wireless connectivity for multimedia services in high speed trains," *IEEE J. Select. Areas Commun.*, vol. 30, no. 4, pp. 729–739, May 2012.
- [5] F. Haider, C.-X. Wang, H. Haas, D. Yuan, H. Wang, X. Gao, X.-H. You, and E. Hepsaydir, "Spectral efficiency analysis of mobile femtocell based cellular systems," in *Proc. IEEE ICCT'11*, Jinan, China, Sept. 2011.
- [6] Y. Zhou, Z. Pan, J. Hu, J. Shi, and X. Mo, "Broadband wireless communications on high speed trains," in *Proc. IEEE WOCN'11*, New Jersey, USA, Apr. 2011, pp.1–6.

- [7] ITU-R M.2135-1, "Guidelines for Evaluation of Radio Interface Technologies for IMT-Advanced," Geneva, Switzerland, Rep. ITU-R M.2135-1, Dec. 2009.
- [8] P. Kyösti, et al., "WINNER II channel models," IST-4-027756, WINNER II D1.1.2, v1.2, Apr. 2008.
- [9] A. Ghazal, C.-X. Wang, H. Haas, M. A. Beach, X. Lu, and D. Yuan, "A non-stationary MIMO channel model for high speed train communication systems," in *Proc. IEEE VTC'12-Spring*, Yokohama, Japan, May. 2012, pp. 347–351.
- [10] S. Knorzner, M. A. Baldauf, T. Fugen, and W. Wiesbeck, "Channel analysis for an OFDM-MISO train communications system using different antennas," in *Proc. IEEE VTC'07-Fall*, Baltimore, USA, Oct. 2007, pp. 809–813.
- [11] N. Kita, T. Ito, S. Yokoyama, Ming-Chien Tseng, Y. Sagawa, M. Ogasawara and M. Nakatsugawa, "Experimental study of propagation characteristics for wireless communications in high-speed train cars," in *Proc. IEEE EuCAP'09*, Berlin, Germany, Mar. 2009, pp. 897–901.
- [12] M. Pätzold and B.O Hogstad, "A wideband MIMO channel model derived from the geometrical elliptical scattering model," in *Proc. IEEE ISWCS'06*, Valencia, Spain, Sept. 2006, pp. 138–143.
- [13] Y. Yuan, A. Ghazal, Q. Yao, and C.-X. Wang, "WP3 report: non-stationary IMT-A MIMO channel model with time-varying AoDs and AoAs," May, 2012.
- [14] X. Cheng, C.-X. Wang, D. I. Laurenson, S. Salous, and A. V. Vasilakos, "An adaptive geometry-based stochastic model for non-isotropic MIMO mobile-to-mobile channels," *IEEE Trans. Wireless Commun.*, vol. 8, no. 9, pp. 4824–4835, Sept. 2009.
- [15] C.-X. Wang, D. Yuan, H.-H. Chen, and W. Xu, "An improved deterministic SoS channel simulator for efficient simulation of multiple uncorrelated Rayleigh fading channels," *IEEE Trans. Wireless Commun.*, vol. 7, no. 9, pp. 3307–3311, Sept. 2008.
- [16] C.-X. Wang, X. Hong, H. Wu, and W. Xu, "Spatial temporal correlation properties of the 3GPP spatial channel model and the Kronecker MIMO channel model," *EURASIP J. Wireless Commun. and Networking*, vol. 2007, Article ID 39871, 9 pages, 2007. doi:10.1155/2007/39871.
- [17] Q. Yao, Y. Yuan, A. Ghazal, C.-X. Wang, L. Luan, and X. Lu, "Comparison of the statistical properties of the LTE-A and IMT-A channel models," in *Proc. IEEE WCNC12*, Paris, France, April 2012, pp. 393–398.
- [18] X. Cheng, C.-X. Wang, H. Wang, X. Gao, X.-H. You, D. Yuan, B. Ai, Q. Huo, L. Song, and B. Jiao, "Cooperative MIMO channel modeling and multi-link spatial correlation properties," *IEEE J. Sel. Areas in Commun.*, vol. 30, no. 2, pp. 388–396, Feb. 2012.
- [19] A. Chelli and M. Pätzold, "A non-stationary MIMO vehicle-to-vehicle channel model based on the geometrical T-junction model," in *Proc. IEEE WCSP'09*, Nanjing, China, Nov. 2009, pp. 1–5.
- [20] A. Chelli and M. Pätzold, "A non-stationary MIMO vehicle-to-vehicle channel model derived from the geometrical street model," in *Proc. IEEE VTC'11-Fall*, San Francisco, USA, Sept. 2011, pp. 1–6.
- [21] C.-X. Wang, X. Cheng, and D. I. Laurenson, "Vehicle-to-vehicle channel modeling and measurements: recent advances and future challenges," *IEEE Commun. Mag.*, vol. 47, no. 11, pp. 96–103, Nov. 2009.
- [22] C.-X. Wang, X. Hong, X. Ge, X. Cheng, G. Zhang, and J. S. Thompson, "Cooperative MIMO channel models: a survey," *IEEE Commun. Mag.*, vol. 48, no. 2, pp. 80–87, Feb. 2010.

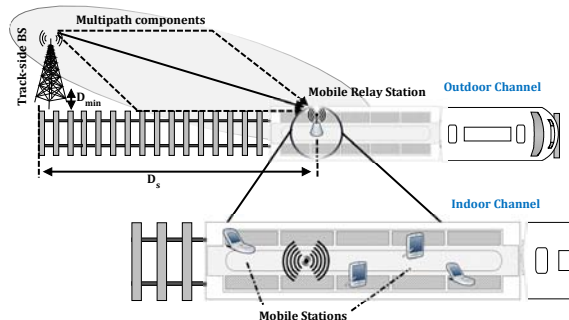


Fig. 1. A HST communication system.

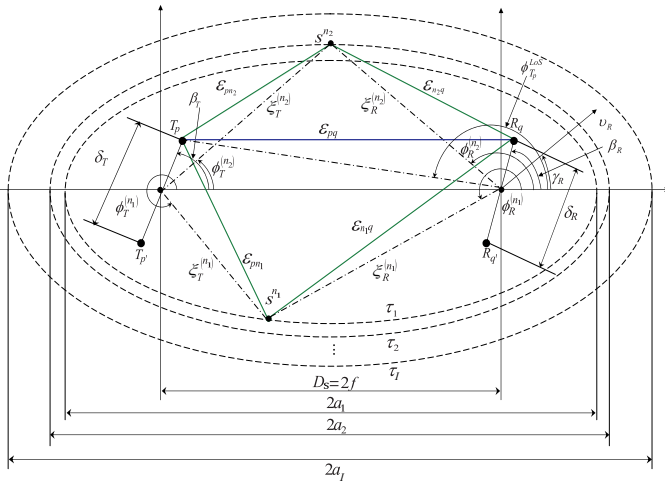


Fig. 2. The GBSM for a MIMO HST channel.

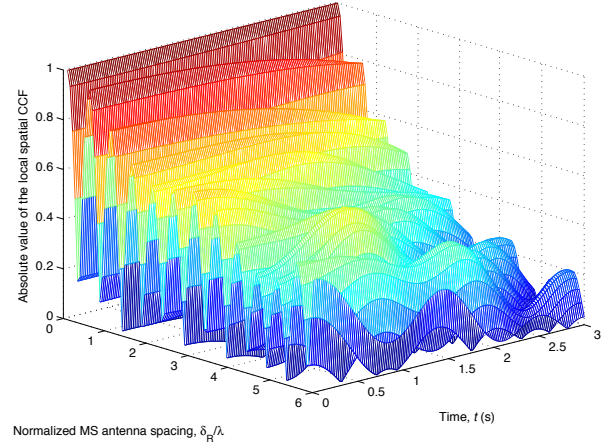


Fig. 5. The absolute values of the local spatial CCF of the second tap of the proposed HST channel model

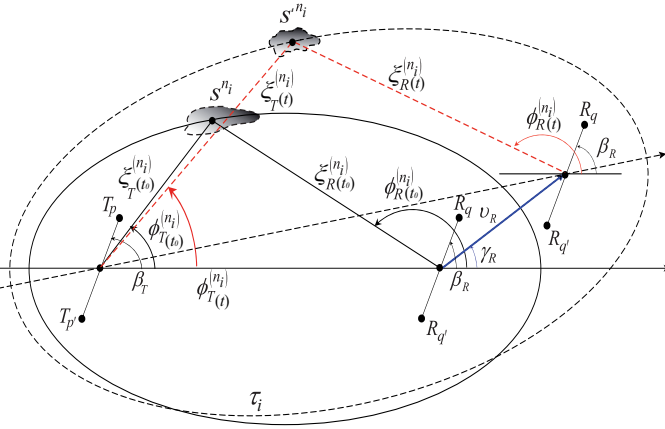


Fig. 3. The time-varying angular parameters in the HST channel model.

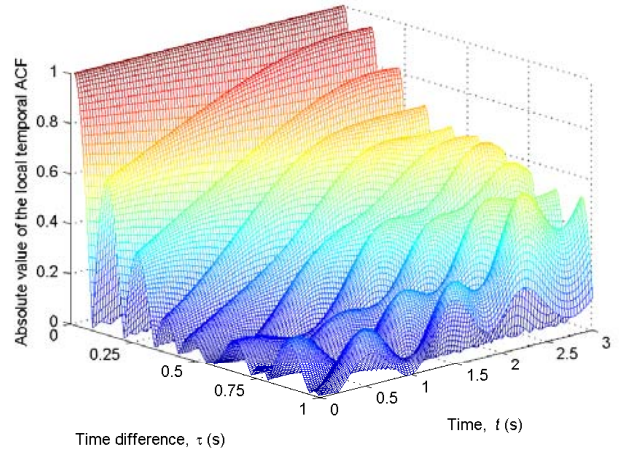


Fig. 6. The absolute values of the local temporal ACF of the first tap of the proposed HST channel model.

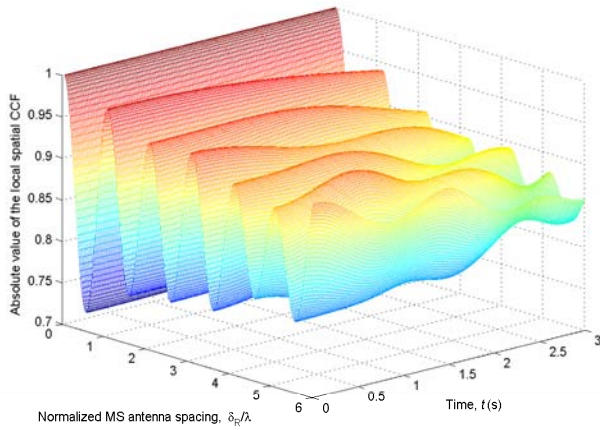


Fig. 4. The absolute values of the local spatial CCF of the first tap of the proposed HST channel model.

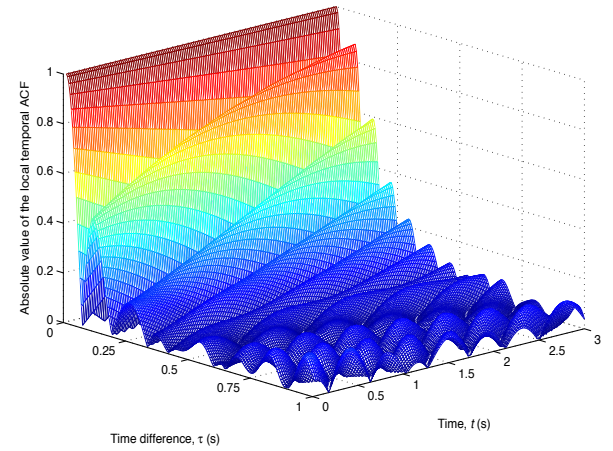


Fig. 7. The absolute values of the local temporal ACF of the second tap of the proposed HST channel model.